Available online at www.sciencedirect.com
ScienceDirect
Sensors and Actuators A 141 (2008) 201–212
SENSORS AND ACTUATORS A PHYSICAL
www.elsevier.com/locate/sna

High flow rate per power electroosmotic pumping using low ion density solvents

Daejoong Kim [a], Jonathan D. Posner [b], Juan G. Santiago [a,*]

[a] *Department of Mechanical Engineering, Stanford University, Stanford, CA 94305, USA*
[b] *Department of Mechanical and Aerospace Engineering, Arizona State University, Tempe, AZ 85287, USA*

Received 5 December 2006; received in revised form 21 July 2007; accepted 23 July 2007
Available online 26 July 2007

Abstract

We present experimental investigations of electroosmotic pumping using porous borosilicate glass and various low ion density liquids. The working liquids were deionized water, deuterium oxide (heavy water), methanol, acetone, acetonitrile and a 1 mM sodium borate buffer as a control. We measured ionic conductivity and, as a useful comparative reference, the zeta potential generated by these liquids in borosilicate microfluidic chips. We evaluated the electroosmotic pump performance of porous borosilicate glass structures in terms of flow rate, pressure and total ionic current. We compared experimental data to an analytical model based on numerical solutions of nonlinear Poisson–Boltzmann equation. In particular, we extend the model to the pumping of pure solvents and found a reasonable agreement with experimental results. For negligible pressure loads, pump flow rate per applied electric power can be more than ten times higher with acetone than with the 1 mM sodium borate buffer. For finite pressure loads, methanol typically yields the highest flow rate per applied electric power due to its higher pressure capacity compared to acetone. Low ion density liquids also showed strong current transients. At present, we do not have a clear understanding of the physics behind these transients, but we present measurements of current startup and discuss possible explanations for the data.

Keywords: Electroosmotic pump; Porous glass; Flow rate per power; Organic solvent; Zeta potential

1. Introduction

Electroosmotic (EO) pumps can generate significant flow rate and pressure differentials in a compact structure with no moving parts. The history of their development was recently reviewed by Yao and Santiago [1]. EO pumps have several potential applications including liquid chromatographic separations [2], miniature drug delivery devices [3], flow injection analysis [4], micromechanical actuators [5], microelectronics cooling [6] and water management in fuel cells [7]. The key figures of merit depend on the specific application and include a pressure, flow rate per unit (device) volume, hydraulic pump work and thermodynamic efficiency. To improve these parameters, various pumping liquids and pumping structures have been used. For example, Reichmuth et al. demonstrated relatively high thermodynamic efficiency using zwitterionic additives [8] and Yao et al. experimentally investigated the use of porous silicon to achieve high flow rate per applied potential [9]. Detailed discussions on these figures of merit can be found in Yao et al. [10], Min et al. [11] and Griffiths and Nilson [12]. One figure of merit of significant interest is the flow rate per applied power, which is particularly important for applications with relatively low pump pressure demands or cases where there is little benefit to increasing working pressure past a minimum required level (e.g., as in drug delivery applications). Another relevant application is water management in fuel cells [7] and the design of methanol pumps for fuel cells [13].

High flow rate per power can be obtained by using low ion density working liquids such as deionized (DI) water or organic solvents. Organic solvents are compatible with EO pumping. They have been used as working electrolytes in various electrokinetic device applications including capillary electrophoresis [14] and electrochromatography [15]. The purposes of using organic solvents (often mixed with water) include (1) the increase in the solubility and stability of analytes (such

* Corresponding author at: Building 530, Room 225, 440 Escondido Mall, Stanford, CA 94305, USA. Tel.: +1 650 723 5689; fax: +1 650 723 7657.
E-mail address: juan.santiago@stanford.edu (J.G. Santiago).

0924-4247/$ – see front matter © 2007 Elsevier B.V. All rights reserved.
doi:10.1016/j.sna.2007.07.023

Nomenclature

a	pore radius (m)
A	cross-sectional area (m^2)
d	distance between an electrode position and a near porous glass surface (m)
D	diffusivity of ions (m^2/s)
e	elementary charge (1.602E−19 C)
F	Faraday's constant (9.649E5 C/mol)
I	current (A)
k	Boltzmann constant (1.380E−23 J/K)
L	length (m)
L_e	distance between electrodes (m)
n	number density (m^{-3})
N_A	Avogadro's number (6.022E23 mol^{-1})
P	electric power (W)
Q	flow rate (ml/min)
r	radius of solvated ions (m)
T	temperature (K)
V	voltage (V)
$\forall$	molal volume (cm^3/g mol)
x	mole fraction
z	valence of ions

Greek symbols

Δp	pressure (Pa)
Λ	molar conductivity of ions (S m^2/mol)
δ	length scale for EDL capacity (m)
ε	permittivity of liquid (F/m)
ϕ	electric potential (V)
η	thermodynamic efficiency
λ	Debye length (m)
μ	viscosity (Pa s)
σ_∞	ionic conductivity (S/m)
τ	tortuosity
ψ	porosity
ζ	zeta potential (V)

Subscripts

app	applied value
eff	effective value
i	ions
liq	liquids
max	maximum value

as lipophilic compounds), (2) the improvement of separation selectivity and efficiency and (3) reduction in analysis time and electric current [16]. Reduction in the electromigration current is especially important in development of high flow rate per power pumps, provided that sufficient flow rate per electric field can be achieved. Wright et al. [17] and Valko et al. [18] measured EO mobility of several pure organic solvents. According to their data, a few organic solvents exhibit EO mobilities comparable to or greater than water.

EO pumping (distinguished from EO flows where no significant pressure is generated) of organic solvents has been reported recently. Chen et al. [19] pumped distilled water, pure methanol and 1:1 methanol/water mixture with silica-based packed capillary columns for high performance liquid chromatography (HPLC). Chang and co-workers [20,21] pumped several aqueous buffers, acetonitrile and methanol using monolithic silica columns for flow injection analyses (FIA) and electrosprays.

In this work, we investigate porous glass EO pumps with high flow rate per power performance using low ion density aqueous solutions and organic solvents. As a comparison, we report zeta potential measurements obtained in glass microchips using the same solvents. We also present selected transient pump performance results. We tested deionized water, deuterium oxide (heavy water), methanol, acetone, acetonitrile and sodium borate buffer (1 mM sodium). We chose these due to their frequent use in various electrokinetic devices and their low ion density.

2. Chemistry of organic solvents

In this section we briefly summarize physical and chemical properties of organic solvents and their effects on electrokinetic phenomena. Organic solvents can be classified by their polarity into nonelectrolytic (associating) and electrolytic (ionic) solvents [22]. Electrolytic solvents can be further classified as protogenic or nonprotogenic solvents. Protogenic solvents donate protons by ionization. Usually, these (protophilic) protons are accepted by another solvent molecule, so that nearly all protogenic solvents are amphiprotic, meaning they donate and accept protons. The self-ionization or autoprotolysis can be expressed as $2HS \rightleftarrows H_2S^+ + S^-$, where S^- represents the deprotonated solvent molecule. Nonprotogenic solvents, also called as aprotic solvents, do not donate protons but sometimes accept protons. Depending on the tendency to accept protons, they can be classified into protophilic, inert or protophobic solvents.

Riekkola et al. [14,18] studied electroosmosis for 16 organic solvents and found that all the solvents that exhibited a measurable zeta potential in a fused silica capillary were either amphiprotic or protophilic. The organic solvents which generated EO flows in their studies are acetonitrile (ACN), acetone, 2-butanone, *N*,*N*-dimethylformamide, *N*-methylformamide, methanol, dimethyl sulfoxide (DMSO), ethanol, formamide, ethyl acetate, tetrahydrofuran, 1-propanol and morpholine in the order of increasing EO mobility. Among these solvents, we chose acetonitrile (electrolytic and protophilic), acetone (electrolytic and protophilic) and methanol (electrolytic and amphiprotic). Table 1 shows the properties of these solvents along with the aqueous solutions we tested. The viscosity and dielectric constant are from Marcus [23] and the remaining values are based on our measurements and model predictions.

3. Theory

In this section, we present an analytical model for porous glass EO pumps and describe how we applied this model to pumping of pure solvents. The model is useful for identifying the

Table 1
Physical and chemical properties of working electrolytes in this study

	μ (mPa s)	ε_r	σ_∞ (S/m)	EO mobility (m^2/V s)	ζ (mV)		λ (nm)
					Inject.	Pump	
Buffer	0.890	78.4	6.2E−3	5.69E−8 ± 1E−10	−73	−96	11
Heavy water	1.12	78.1	1.2E−3	4.5E−8 ± 3E−9	−71	−77	42
DI water	0.890	78.4	2.4E−4	4.77E−8 ± 1E−10	−61	−64	120
Methanol	0.551	32.7	8.9E−5	3.7E−8 ± 6E−9	−69	−74	180, 85
Acetone	0.303	20.6	9.4E−6	4.62E−8 ± 9E−10	−76	−50	580, 260
Acetonitrile	0.341	35.9	1.8E−5	6.7E−8 ± 8E−9	−72		360, 210

Note: Viscosity and dielectric constant from [23]. We assumed the same viscosity and dielectric constant for buffer and DI water. As explained in Section 3, we estimated organic solvent pumping, using two approaches: Nernst–Einstein equation, combined with Scheibel's empirical relation (left-hand column) and Stokes's law with estimated ion size (right-hand column).

optimal high flow rate per power solvent for a given pump/load application.

3.1. Analytical model for porous glass EO pumps

Yao and Santiago presented an analytical model for EO pumping in porous materials by treating the media as an array of cylindrical microchannels of uniform pore radius, a, with tortuosity, τ and porosity, Ψ [1]. This model was based on the solution of Poisson–Boltzmann equation with assumptions of uniform and constant zeta potential, viscosity and dielectric constant. For both symmetric and general electrolytes, the flow rate, Q, depends on the applied potential, V_{app} and pressure, Δp, as

$$Q = \frac{\psi}{\tau}\left[-\frac{\Delta p A a^2}{8\mu L} - \frac{\varepsilon\zeta A V_{eff}}{\mu L} f\right], \tag{1}$$

where ε and μ are the permittivity and viscosity of liquids, respectively, A and L the cross-sectional area and thickness of porous materials, respectively, and ζ is the zeta potential. The effective potential, V_{eff}, is ζ the effective potential applied across the pumping material. To estimate V_{eff}, we subtract from V_{app} the external potential required to initiate electrolytic reactions and the estimated potential associated with ohmic loss between electrodes and the substrate.[1] The function f is defined as

$$f = \int_0^a \left(1 - \frac{\phi}{\zeta}\right)\frac{2r}{a^2}\,\mathrm{d}r, \tag{2}$$

where ϕ is the electric potential, which can be obtained by solving the Poisson–Boltzmann equation.

Key figures of merit for EO pumps are the maximum flow rate, current and pressure, respectively, given as,

$$Q_{max} = -\frac{\psi\varepsilon\zeta A V_{eff} f}{\tau\mu L}, \tag{3}$$

$$\Delta p_{max} = -\frac{8\varepsilon\zeta V_{eff} f}{a^2}, \tag{4}$$

$$I_{max} = \frac{\sigma_\infty \psi A V_{eff} f}{\tau L g}. \tag{5}$$

For electroosmotic pumping of a solution containing N ionic species, g can be defined as

$$g = \frac{f}{\int_0^a [\varepsilon^2/\mu\sigma_\infty(\mathrm{d}\phi/\mathrm{d}r)^2 + (1/\sum_{i=1}^N x_i\Lambda_i) \times \sum_{i=1}^N x_i\Lambda_i \exp(-z_i e\phi/kT)](2r/a^2)\,\mathrm{d}r}. \tag{6}$$

This relation includes the contributions to total current from advective charge transport (first term) and electromigration (second term) and neglects contributions from diffusive fluxes (very reasonable for electroosmotic pumps) [1]. σ_∞ is the ionic conductivity of liquids and z_i, x_i and Λ_i, respectively, the valence number, mole fraction and molar conductivity of ion i. k is the Boltzmann constant, T the temperature of liquids and e is the elementary charge. f and g both vary between zero and one (see inset of Fig. 6) and take into account the effects of finite electric double layers (EDLs). They strongly depend on the ratio of pore radius a and the Debye length given by,

$$\lambda = \left(\frac{\varepsilon kT}{e^2\sum_{i=1}^N z_i^2 n_i}\right)^{1/2}, \tag{7}$$

where n_i is the bulk electrolyte ion number density of species i. By "bulk," we here refer to the ion densities outside of the double layer. f and g of unity imply thin EDLs, where the EO velocity can be expressed by the Helmholtz–Smoluchowski relation $u_{EO} = -\varepsilon\zeta V_{eff}/\mu L$. A detailed explanation of f and g is given in Yao and Santiago [1]; these parameters are determined by numerically solving the nonlinear Poisson–Boltzmann equation. (In the special case of the Debye–Hückel limit of low zeta potential and for monovalent, symmetric electrolytes, their analytical forms are given in Eqs. (6) and (25) in Yao and Santiago [1].)

Combining these equations results in several relations useful for various EO pump applications. The maximum flow rate

[1] The external potential required to initiate electrolytic reactions is the theoretical potential for electrolysis plus an empirically determined overpotential which depends on surface chemistry, electrolyte and current density, among other factors [24,25]. We estimate this potential as that associated with extrapolating the linear (ohmic) regime of the measured current versus potential curve to the zero current axis. The (empirical) zero current extrapolations for deionized water, deuterium oxide (heavy water), methanol, acetone, acetonitrile and sodium borate buffer (1 mM sodium) are 7.3, 6.1, 2.9, 6.1 and 5.4 V, respectively. These values may have a slight (consistent) bias due to the measurement procedure but this should not affect our estimate of electric field and V_{eff} in the fully ohmic region. We also note that the relatively small value for methanol is consistent with the data of Narayanan et al. [26], who present measurements of the electrolysis of methanol. See Kim et al. [27] for a similar discussion on aqueous solutions.

per current (the key parameter of this work) and the ratio of maximum flow rate to maximum pressure can be, respectively, expressed as,

$$\frac{Q_{\max}}{I_{\max}} = -\frac{\varepsilon\zeta g}{\mu\sigma_\infty}, \tag{8}$$

$$\frac{Q_{\max}}{\Delta p_{\max}} = \frac{\psi A a^2}{8\tau\mu L}. \tag{9}$$

The latter is useful in estimating the pore radius of porous materials since porosity is easily measured with wet/dry weighing (and tortuosity does not, in our experience, vary much from 1.45 for these frits). Note that Eq. (9) is only a function of viscosity when all the geometric parameters of porous materials are fixed. Another key parameter is the thermodynamic efficiency, defined as $\eta = Q\,\Delta p/(V_{\text{app}} I)$, given by

$$\eta \approx \frac{1}{2}\frac{Q_{\max}\,\Delta p_{\max}}{I_{\max} V_{\text{eff}}} = 8\frac{\varepsilon^2}{\mu}\frac{\zeta^2}{\sigma_\infty}\frac{1}{a^2} fg. \tag{10}$$

We again stress the importance of appropriate figures of merit for different applications. η is a fundamental parameter, but not always of primary interest.

3.2. Estimating EO pumping performance of pure solvents

Ion density and valence information is required to evaluate Eq. (6). In some simple cases (e.g., where ion mobilities in a binary electrolyte are known), ion density can be determined from ionic conductivity measurements and $\sigma_\infty = \sum_{i=1}^{N} n_i \Lambda_i / N_A$ (where N_A is the Avogadro's number). (The molar conductivity Λ_i, of common ions in water is tabulated in, for example, the CRC Handbook [28].) However, this approach is typically not possible in the case of organic solvents as the mobility and valence of all ions are not easily identified. Below, we propose two ways to estimate a relation between ion density and (measured) conductivity for such solutions. We used these estimates of molar conductivities to estimate ion densities and, in turn, to estimate Debye length and compute the values of f and g. These molar conductivities were not used to predict Joule-type ion conductivity (the major source of current transport and power loss) as total ionic conductivity was a quantity we measured directly.

In modeling EO pumping of DI water, we assume that carbonic acid dominates the ionic conductivity. Water becomes saturated with carbon dioxide, when exposed to the atmosphere [29]. Dissolved carbon dioxide reacts with water, forming carbonic acid: $CO_2(aq) + H_2O \rightleftarrows H_2CO_3(aq) \rightleftarrows H^+(aq) + HCO_3^-(aq)$. (The typical measured pH of our DI water is ~5.2.) We estimated the ion density of DI water by assuming that its conductivity is due solely to carbonate, HCO_3^- and hydronium ions (i.e., we relate the mobility of these two ions to the measured conductivity, and thereby deduce total ion density). Table 1 shows the resulting estimate of Debye length as well as the measured ionic conductivity.

We performed pump experiments with heavy water. We took care not to overly expose this electrolyte to the atmosphere (e.g., we used N_2 purged reservoirs as described in Section 4), but the relatively high value of conductivity of our heavy water samples indicates significant concentrations of impurity ions.[2] For the purpose of estimating Debye length and the parameters f and g, we therefore again assumed the mobility of carbonic acid ions. We estimated the molar conductivity of carbonic acid ions in heavy water from that in water using Walden's rule [30],

$$\Lambda_i \mu = \frac{z_i e F}{6\pi r_i} = \text{constant}, \tag{11}$$

where F is the Faraday's constant and r_i is the radius of a solvated ion. Walden's rule assumes a uniform radius r_i of ion i solvated in water and heavy water in this case. This assumption may not be appropriate for organic solvents [30] but we believe that this is a reasonable assumption for heavy water due to its chemical similarity to water [23].

For estimating the Debye lengths (and functions f and g) of the organic solvents used here, we propose the use of mass spectrometry data to identify likely solvated ions and thereby establish the relation between (measurable) conductivity and ion density (required to predict f and g). Mass spectrometry data are available for numerous organic solvents [31–33], and can be classified into two types: for cations and anions. Typically, mass spectrometry data present the abundance of each ion relative to the most abundant ion which is assigned an abundance of 100% [34]. The number of ion types reported is often fairly large (e.g., 27 cations for acetone mass spectrometry) and many of the ions are present in only trace quantities that contribute negligibly to conductivity estimates. For simplicity, we include here only major ions defined as follows: We start with the most abundant ion, we then progressively include the next abundant ion species until our estimates of f and g change by less than 5%. This process yields the relatively brief list of relevant ions summarized in Table 2. We categorize these as major cations and anions for each solvent and we have re-scaled the relative abundance of each ion such that their sum is again normalized to 100%.

After estimating ion type and relative abundance from mass spectrometry, we estimated the molar conductivity of each ion using two approaches suggested by work in the electrochemical field. For each of these, we are forced to make a few assumptions, and the respective molar conductivity and Debye length value of each should therefore be interpreted as an order of magnitude estimate.

In the first approach, we used Scheibel's empirical formula to estimate diffusivity [35],

$$D_i = 8.2 \times 10^{-15}\frac{T}{\mu}\frac{1 + (3\forbar_{\text{liq}}/\forbar_i)^{2/3}}{\forbar_i^{1/3}}, \tag{12}$$

where $\forbar_i$ is the molal volume of ions and $\forbar_{\text{liq}}$ is the molal volume of liquids, both in $\text{cm}^3/\text{g mol}$. For $\forbar_i$, we used Le Bas's

[2] D^+ and OD^- ions alone are unlikely to explain the measured value of conductivity. We expect the dissociation of heavy water, expressed as $D_2O \rightleftarrows D^+ + OD^-$ to yield ion densities on the order of 0.1 μM (as in the case of water). Assuming this theoretical minimum ion density and molar conductivities of D^+ and OD^-, the ionic conductivity would be roughly 10 times lower than measured.

Table 2
Assumed ion contents in each solvent and estimated molar conductivities for major cations and anions

	Cations	Λ_i (m^2 S/mol)	Anions	Λ_i (m^2 S/mol)
Buffer	Na^+	5.0E−3	1/2 $B_4O_7{}^{2-}$	2.5E−3
Heavy water	D^+	2.0E−2	$DCO_3{}^-$	3.5E−3
DI water	H^+	3.5E−2	$HCO_3{}^-$	4.4E−3
Methanol	47% CH_2OH^+	1.7E−2, 6.4E−3	71% O^-	6.1E−2, 1.1E−2
	34% CHO^+	2.0E−2, 7.0E−3	15% OH^-	4.2E−2, 9.3E−3
	19% $CH_3{}^+$	2.0E−2, 7.0E−3	14% CH_3O^-	1.7E−2, 6.4E−3
Acetone	75% CH_3CO^+	3.1E−2, 1.0E−2	41% O^-	1.7E−1, 1.9E−2
	17% $CH_3{}^+$	5.3E−2, 1.3E−2	26% CHC^-	4.3E−2, 1.2E−2
	8% CH_2CO^+	3.4E−2, 1.1E−2	21% $CHCO^-$	3.6E−2, 1.1E−2
			12% $C_2{}^-$	4.7E−2, 1.2E−2
Acetonitrile	73% CH_2CN^+	2.3E−2, 8.9E−3	77% CN^-	3.6E−2, 1.1E−2
	27% $CHCN^+$	2.4E−2, 9.1E−3	23% $CHCN^-$	2.4E−2, 9.1E−3

Note: We present two different values of Λ_i for organic solvents: Nernst–Einstein equation, combined with Scheibel's empirical relation (left-hand column) and Stokes's law with estimated ion size (right-hand column).

additive method [36].[3] Given information of the diffusivity, we then estimate the molar conductivity of each ion using the Nernst–Einstein equation [30],

$$\Lambda_i = \frac{z_i e F}{kT} D_i. \tag{13}$$

Table 2 summarizes the molar conductivities of all the individual ions. In order to apply these values to Eq. (6), we approximate x_i as the ion abundance fraction from mass spectrometry data.

The second approach of estimating the molar conductivity of each ion is to estimate the characteristic ion radius using the empirical relation [37],

$$r_i = 0.72 \times 10^{-10} V_i{}^{1/3}. \tag{14}$$

This relation was originally developed for (typically uncharged) liquid molecules but we hypothesize that it should yield an appropriate order of magnitude for ion length scales. Substituting r into Stokes's law [37], we obtain

$$\Lambda_i = \frac{z_i F^2}{6\pi N_A \mu r_i}. \tag{15}$$

Table 2 shows a summary of the results from these two methods; both yield similar estimates for f and g.

We can now estimate the flow rate per power pumping of various solvents, using the parameters listed in Tables 1 and 2. For negligible pressure loads, flow rate per power scales with applied voltage as follows: $Q/P = Q_{max}/I_{max}V_{app} = -\varepsilon\zeta g/\mu\sigma_\infty V_{app}$ (e.g., see the experimental data in Fig. 5). In the more general case with finite pressure loads, flow rate per power can be expressed as follows:

$$\frac{Q}{P} \approx \frac{Q}{\sigma_\infty(\tau/\psi)(L/A)(1/f)(\mu/\varepsilon\zeta)^2 \times (Q + \Delta p(1/8)(\psi/\tau)(1/\mu)(A/L)a^2)^2}. \tag{16}$$

[3] Scheibel's empirical formula was originally proposed for nonelectrolytes and Le Bas's additive method for pure liquids.

Here, we explicitly retain pressure load Δp and flow rate as these are often design parameters of interest. Fig. 1 shows Q/P from Eq. (16) for sodium borate buffer (1 mM sodium concentration), DI water, methanol and acetone. For these plots, we calculate the molar conductivity of methanol and acetone using the first approach (Nernst–Einstein equation combined with Scheibel's empirical formula). We used measured values of conductivity to predict the electromigration component of current (i.e., we measure σ_∞ directly) [1]. We here show a plot of dimensional Q/P versus (dimensional) pressure load, with flow rate and solvent type as parameters. This plot is most useful in the practical design of an EO pump with a finite pressure load; and in particular in choosing a solvent given a dimensional pressure and flow rate requirement. The plot shows data sets for two example design flow rates of 0.002 and 2 ml/min. (Note Q is the expected flow rate for a coupled pump and load system and not the maximum achievable pump flow rate.) For each set of curves, applied voltage is varied so as to hold the flow rate constant. For $Q = 0.002$ ml/min, the voltage ranges for buffer, DI water, methanol and acetone are, respectively, 24–36,

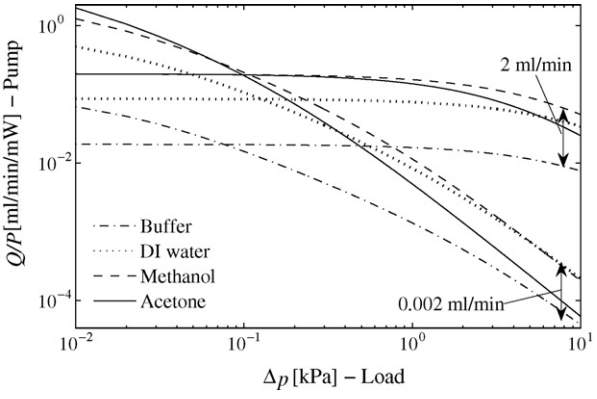

Fig. 1. Model prediction of EO pump performance for different solvents and varying pump loads and flow rate. Geometry of porous glass materials is given in Section 4 and the solvent properties are given in Tables 1 and 2. There are two flow rate ranges fixed at 0.002 and 2 ml/min. The flow rate per power at the minimal load is in the order of buffer, DI water, methanol and acetone. This order changes as the voltage required for the flow rate constraint changes.

39–62, 55–110, 120–330 V. For $Q = 2$ ml/min, the voltage ranges for buffer, DI water, methanol and acetone are, respectively, 4.2–17, 4.2–26, 4.2–56, 4.3–220 V. Fig. 1 highlights the importance of correctly matching a working liquid for a given load and flow rate. At very low pump loads, 1 mM borate buffer, DI water, methanol and acetone have increasingly higher flow rate per power performance at either flow rate. However, the optimal value of flow rate per pump power is a function of pump load and flow rate. For example, pump loads of approximately 0.1 kPa favor methanol over acetone for both of the design flow rates. These Q/P crossovers by different working electrolyte curves are a weak function of design flow rate (e.g., 0.06 kPa for $Q = 0.002$ ml/min and 0.07 kPa for $Q = 2$ ml/min). For greater than ~0.07 kPa loads, about three times higher voltage is required for acetone versus methanol in order to achieve the required flow rate, resulting in higher power demands for an acetone system. The curves for $Q = 0.002$ ml/min condition show the crossover favoring DI over methanol for loads greater than 5 kPa. In the next section, we present an experimental validation of this model, with an emphasis on high flow rate per power pumping at minimal loads.

4. Experimental

In this section, we investigated the effects of the working liquid chemistry on flow rate per power. We describe the experimental setup used to measure the ionic conductivity and the zeta potential as well as the structure of EO pumps and the experimental setup used to characterize the pump performance. The working liquids were DI water, heavy water (deuterium oxide), methanol, acetone, acetonitrile and sodium borate buffer (1 mM sodium concentration) as a reference. We did not use acetonitrile in our EO pump experiments as we were concerned with the possible production of cyanide during electrolysis of acetonitrile (CH_3CN, methyl cyanide). Note that our ionic current values and associated molar rates of acetonitrile electrolysis would be orders of magnitude larger than in typical capillary-based electrokinetic experiments.

4.1. Solvent chemistry

We purchased DI water (W2-20 deionized ultra-filtered water) from Fisher Scientific (Hampton, NH, USA) and prepared 1 mM buffer solution by dissolving sodium borate powder ($Na_2B_4O_7$, J.T. Baker, Phillipsburg, NJ, USA) in DI water. We used heavy water (99.96% atom D) from Sigma–Aldrich (St. Louis, MO, USA). All of the organic solvents are of HPLC grade also from Sigma–Aldrich with reported purity greater than 99.9%. In all the experiments, we use the solvents as delivered to us without further purification.

Ionic conductivity for borate buffer, DI water and heavy water was easily measured with a conductivity meter (Corning Pinnacle 542 pH/conductivity meter, Corning, NY, USA). For the low conductivity solvents, such as methanol, acetone and acetonitrile, we measured conductivity by measuring current in a 100 μm diameter round capillary (VitroCom, Mountain Lakes, NJ, USA). For the latter work, we begin each experiment by flushing the solvent of interest for 30 min using a vacuum pump. We then apply an electric potential to two platinum electrodes immersed in the two channel end reservoirs. We apply voltages of order 100 V (for order 10 V/cm fields) and measure the sourced current using a sourcemeter (Keithley 2410 1100 V Sourcemeter, Cleveland, OH, USA). We calculate ionic conductivity from the current per applied voltage slope, I/V_{app}; measurements are well into the ohmic conduction regime but with current densities such that Joule heating was negligible. Conductivity is then $\sigma_\infty = (I/V_{app})(L/A)$, where V_{app} is the applied potential, I the measured current and L and A are the length and the cross-sectional area of the capillary, respectively.

As a basis of comparison, we performed microchip-based electrokinetic injection experiments to measure the zeta potential. We used a cross-pattern borosilicate microchip with isotropically etched microchannels (Micralyne PC-SC microfluidic chip, Edmonton, Alta., Canada). The chip material has a similar glass composition as the porous glass frit (see below) although such measurements should be interpreted as an approximate predictor of zeta potential in the porous glass frit systems. For zeta potential measurements, we initially evaluated the applicability of the current monitoring technique described by Huang et al. [38]. However, we found two major difficulties with applying this technique to pure solvents. First, the ionic current of pure solvents was often prohibitively low (order of 1 nA at 1 kV with acetone in a 10 cm long, 100 μm diameter capillary), giving a low signal-to-noise ratio for the measurement. Secondly, this method requires precise (small percentage) adjustments of electrolyte conductivity but in a manner which is not expected to change wall charge (and this issue is not well understood for low conductivity solvents). We chose electrokinetic injection experiments with a microfluidic chip and tracking of neutral fluorescent dyes as a basis for electroosmotic mobility measurements. This experimental procedure is described in, for example, Jacobson and Ramsey [39]. The overall experimental setup for these experiments is the same as in Posner and Santiago [40], except that we implemented some changes to the voltage scheme. We visualized the EO flow in the chip using an epifluorescent microscopy with a Rhodamine B, a neutral fluorescent dye (Acros Orgaincs, Geel, Belgium).

4.2. EO pump experimental setup

We use borosilicate porous glass frits as the EO pumping (Ultrafine, ROBU Glasfilter-Geraete GmbH, Hattert, Germany). These frits have been characterized in Yao et al. [10]. The frit used in this work was 4 cm in diameter and had an area-average thickness of 4.78 mm. We measured the porosity as 0.20 by weighing dry and wet samples using a microbalance (ACCULAB, Newtown, PA, USA). We assume the tortuosity was 1.45, a typical value for these ROBU ultrafine porous glass frits [10]. We estimated the pore radius a to be 0.68 μm using Eq. (9) and experimentally determined maximum flow rate and maximum pressure with the buffer. There are other ways to estimate a pore radius: These include measurement using a porosimeter, analyses of scanning electron microscope (SEM) images, and measurements of hydraulic resistance (using Darcy's law). Brask

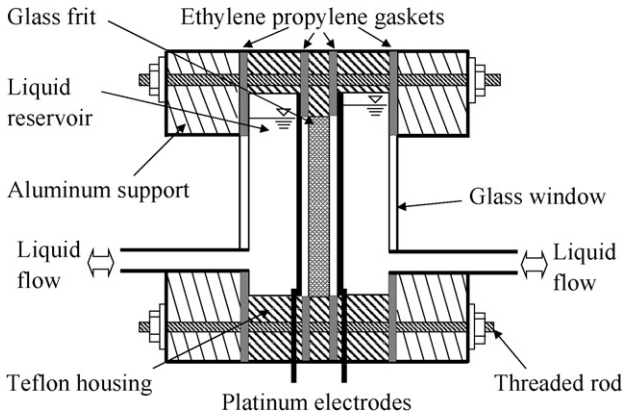

Fig. 2. Schematic of the EO pump device. Pump housing is machined from Teflon to allow flexibility in working liquids and fitted with a glass window. All the components touching liquids are inert to strong solvents, such as acetone. DC or AC voltages can be applied.

et al. compared the latter two with our method and recommended the use of Eq. (9) for EO pump modeling [41].

Fig. 2 shows the schematic of the EO pump. The basic functionality of this pump is similar to others used for aqueous solutions [10], but we here used housing and sealing materials compatible with strong solvents such as acetone. We fabricated pump housings using poly-tetra-fluoro-thylene (PTFE) and sealed these with ethylene propylene O-rings and a special adhesive (3M 2216, St. Paul, MN, USA). To achieve a good seal, the pump is compressed using machined aluminum supports with glass windows. All the components in contact with working liquids were inert to strong solvents. The electrodes were spiral wound platinum wires (approximately 10 cm), positioned about 1 mm from the frit. The 1.42 mm inner diameter outlet tubes were PTFE.

Fig. 3 shows the experimental setup for flow rate and current measurements. We drive the EO pump with low frequency square wave voltage signals (0.02–0.1 Hz) that are generated with a data acquisition (DAQ) card (National Instruments PCI-6220, Austin, TX, USA) and amplified with a voltage amplifier (Trek PZD350, Medina, NY, USA). This low frequency (near-DC) forcing functions are convenient for long-term experiments and allow us to incorporate, for example, controlled atmosphere

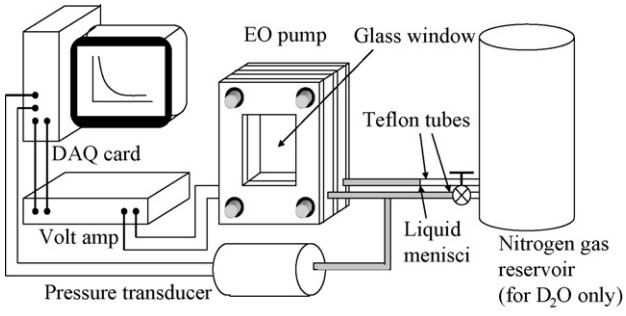

Fig. 3. Experimental setup for flow rate and current measurements. Liquid is pumped using an AC field of low frequency. In the case of heavy water measurements, outlet tubes were connected to a 250 cm^3 reservoir with a nitrogen gas cap. For pressure measurements, one of the outlet tubes was connected to a pressure transducer.

reservoir experiments (e.g., see Fig. 3). We connected the pump outlet tubes to a 250 cm^3 reservoir filled with inert nitrogen gas to prevent solvent evaporation and, more importantly, to prevent long-term absorption of atmospheric gases (e.g., heavy water is very hygroscopic). Since the frequency was quite low, we expect roughly DC mode pumping after short-term transient operation. We further discuss current transients and long-term stability below.

We measured the flow rate by determining the time required for the leading edge of an air bubble to travel a set distance along one of the outlet tubes. We measured the current with the DAQ card by measuring the voltage drop across a known resistor connected to the pump in series. To measure the maximum pressure, we sealed one end of tube with a pressure transducer (Omega PX303-015G5V, Stamford, CT, USA), and collected the signal with the DAQ card. New frits often show higher-than-expected conductance values (we assume this is due to impurity ions desorbing from the material). To mitigate this, we first cleaned the frits with DI water using combined pressure-driven and EO flows for 24 h or more. In addition to this initial cleaning process, we ran the EO pump with the solvent of interest for at least 4 min a minimum of five times, before each set of experiments.

5. Results and discussion

In this section, we present measurements of ionic conductivity and zeta potential for all our working liquids, followed by measurements of maximum flow rate, maximum pressure generation and maximum current for pure solvents. We compare the experimental results with the analytical model and present current transients data for low ion density liquids.

5.1. Measured solvent properties

The measured working electrolyte ionic conductivity values are shown in Table 1.[4] Table 1 also shows Debye length estimations based on the mass spectroscopy model described earlier and zeta potential measurements for the borofloat microchannels. As described in Section 3, we used two methods to estimate the representative molar conductivity for cations and anions for organic solvents and, accordingly, present two values for the Debye length for methanol, acetone and acetonitrile. Again, these pure solvent Debye length estimations should be taken as a rough approximation. The Debye length estimation for DI water is reasonably accurate as the measured pH of 5.2 is consistent with the proton concentration estimated by the ionic conductivity measurement. The increasing order of the zeta potential in our measurements coincides with that reported by Valko et al. [18] as follows: acetone, acetonitrile, heavy water, methanol and

[4] We included heavy water here as a test working liquid as the ion mobilities of D^+ and OD^- are smaller than H^+ and OH^- [28]. However, we found that, for both water and heavy water, conductivity is dominated by impurities and not these inherent ions. As such, conductivity and EO performance is dominated by purification and treatments such as deionization, distillation and their exposure to atmospheric gases. We conclude that there is therefore no practical advantage in using heavy water given the figures of merit explored here.

water. However, the absolute values we measured are roughly half of those in Valko et al. for all the pure solvents. We attribute this discrepancy to the fact that our surface material is different: we used borofloat microchips, while Valko et al. used fused silica capillaries (all of which had different pre-experiment surface treatments). Valko et al. also used a DI water injection plug as a marker with an ultraviolet (UV) detection, while we used a Rhodamine B dye of 1 μM concentration, an approximately neutral marker. Further, although Valko et al. and our experiments both used HPLC grade organic solvents, impurity ions in these solvents may be different due to supplier variations and experimental procedures.

5.2. EO pumping experiments

Fig. 4 summarizes our measurements of flow rate, current and pressure for an applied voltage range from 10 to 100 V. For acetone we applied larger voltages of 50–350 V to obtain flow rates commensurate with the other solvents. The flow rate, pressure and current are a linear function of the applied voltage, as expected. The error bars denote 95% confidence limits as per the *t*-distribution. For flow rate and current, these were based on the ensemble average of data in four realizations, while those for pressure were based on the time average of data in a single realization. Fig. 5 shows the flow rate normalized by pump power. As a validation of the trend predicted by the model, we show, with the measured data, predictions of plotted flow rate per power, $Q_{\max}/(V_{\text{app}}I_{\max})$ (solid curves). For this, we use the maximum flow rate per current expression from Eq. (8), with the product ζg as a fitting parameter. The fit values for ζg are −0.10, −0.042, −0.0067, −0.018 and −0.0042 V for buffer, heavy water, DI water, methanol and acetone, respectively. These can be compared to the respective values of −0.060, −0.040, −0.017, −0.030 and −0.0061 V determined from the on-chip measurements of ζ (a similar but clearly different surface) and the model predictions of g. The curve shape closely follows the expected V_{app}^{-1} dependence and the independently determined ζg values are fairly close to the observed values.

Fig. 5 shows that acetone shows the best (negligible pressure load) performance with more than ten times higher flow rate per power than the buffer. The flow rate per power in the increasing order is given as acetone, methanol, DI water, heavy water and the buffer. This order is the same as for the model prediction of flow rate per power with zero pump load, shown in Fig. 1. Although not shown here, the pressure normalized by power shows the same order as well. We estimated thermodynamic efficiency using the measured $Q_{\max}$, $I_{\max}$ and $\Delta p_{\max}$ in Eq. (10); the resulting values are 0.24, 0.30, 0.21, 0.41 and 0.22% for buffer, heavy water, DI water, methanol and acetone systems, respectively. The increasing order of thermodynamic efficiency for different solvents does not coincide with the order for flow rate per power. That is, although low conductivity can lead to significantly high values of flow rate per power, low ion density also leads to relatively low values of hydraulic power output due to finite EDL effects. Eq. (10) shows that the thermodynamic efficiency depends linearly on the product of f and g, meaning that finite EDL effects are more important on thermodynamic

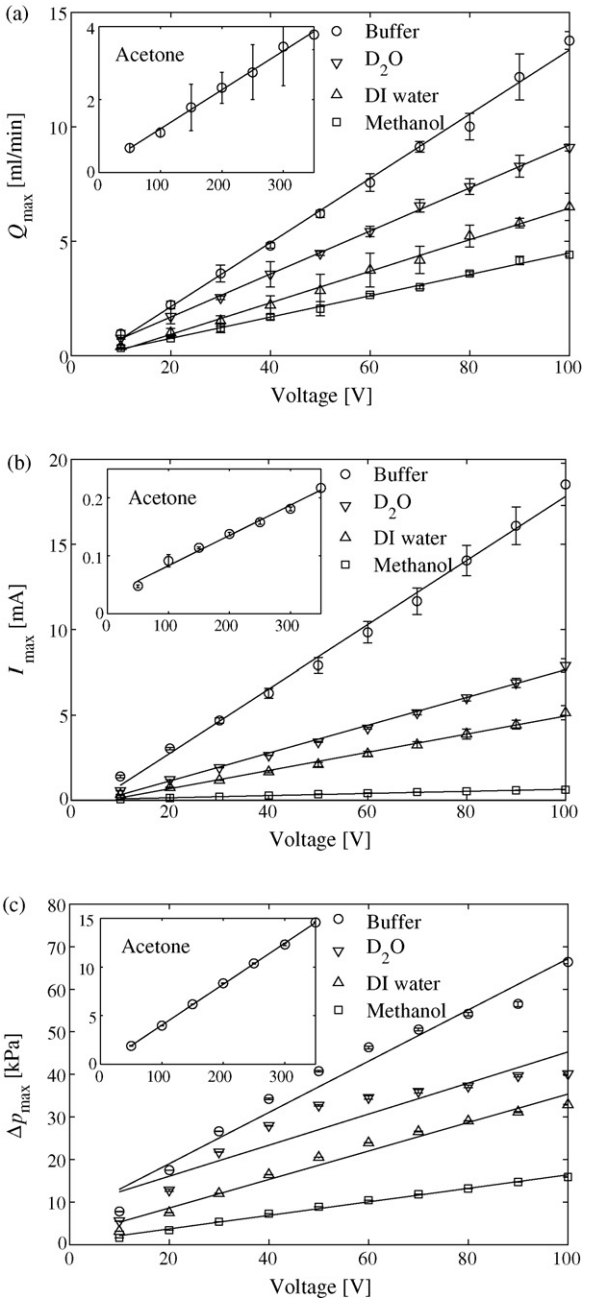

Fig. 4. Flow rate, current and pressure vs. applied voltage for all the working liquids. Inset shows extended voltage range for acetone. The error bars for flow rate and current were estimated from multiple realizations and those for pressure were from time-averaging of single realizations.

efficiency than on flow rate per power. (Absolute optimization of thermodynamic efficiency, a problem not explored here, would entail variation of pore diameter.) Another point on thermodynamic efficiency estimates is that these values are relatively low, e.g., compared to 0.3% for buffer and 1.3% for DI water, maximum values reported by Yao et al. [10] and Zeng et al. [42], respectively. This is most likely due to the relatively large pore radius used here (efficiency scales as a^{-2} in Eq. (10)).

In Fig. 6, we compare the model predictions and experimental values for f and g, to validate our model as well as to confirm finite EDL effects. We obtained empirical estimates of f and g

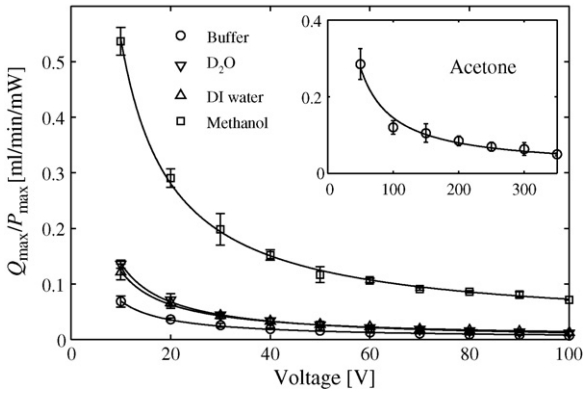

Fig. 5. Flow rate per power for all the working liquids. Inset shows extended voltage range for acetone. The error bars were estimated from multiple realizations. The solid curves are trend predictions obtained using Eq. (8) with ζg as a fitting parameter.

from $f = -Q_{\max}\tau\mu L/\Psi\varepsilon\zeta A V_{\text{eff}}$ and $g = -(Q_{\max}/I_{\max})\mu\sigma_\infty/(\varepsilon\zeta)$, which are rearranged forms of Eqs. (3) and (8), respectively. For these estimates of f and g, we used the zeta potential values from the on-chip injection experiment (as a completely independent estimate), along with other solvent properties listed in Table 1. The two approaches for f and g estimation described earlier result in the data shown in Fig. 6a and b. Note that $a^* \equiv a/\lambda$ for pure solvents is different for the two approaches since the Debye length estimates are different. The inset in Fig. 6a shows

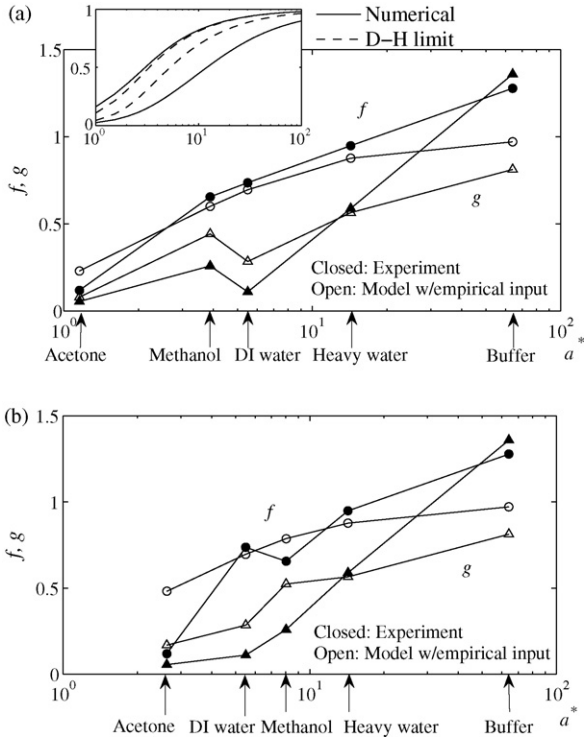

Fig. 6. Finite electric double effects expressed as f and g for all the working liquids from the analytical model (open symbols) and the experiments (closed symbols). (a) We used Nernst–Einstein equation, combined with Scheibel's empirical relation. (b) We applied Stokes's law with estimated ion size. Inset shows dimensionless numbers, f and g, against the pore radius relative to Debye length. For this calculation we assumed parameters only for the buffer, so f and g predictions for other liquids should be different, although trends are similar.

the trend for f and g in the buffer versus a^*. In Fig. 6, we confirm that the finite EDL effects become greater (f and g approach zero) as the ion strength decreases (a^* decreases). Both of the experimental and model values show a trend similar to the plot in the inset and agree reasonably well. However, the approximations used here do show some important discrepancies. Most importantly, estimated f and g values for the borate buffer exceed unity (which is unphysical). This discrepancy is mostly due to the fact that zeta potential in the porous glass EO pumps is most likely different than that of the borofloat microchips. Yao et al. [10] reported approximately −100 mV zeta potential for the same buffer and with similar frit materials. This value is 27% higher than the value from our on-chip experiments. This difference in zeta potential values is shown in Table 1, where we present zeta potential estimates from on-chip data and from the frit experiments (and Eqs. (2) and (3)). (We estimate these values in a self-consistent fashion, i.e., satisfying Eq. (2) for f and Eq. (3) for experimental $Q_{\max}$, simultaneously.) As shown in Table 1, the zeta potential from two methods can be different (up to ∼50% for acetone).

Despite the discrepancies, the model is useful in explaining trends in applied voltage and differences across working liquids. For example, $Q_{\max}/V_{\text{app}}$ values (e.g., slopes of curves in Fig. 4a) for each solvent are roughly in increasing order of their EO mobility as predicted from the borosilicate chip system measurements (see Table 1), except for acetone. For acetone, EO mobility is similar to that of the buffer but the maximum flow rate with acetone is significantly smaller than with the buffer. This large deficit of flow rate is qualitatively captured by model through the factor f (0.97 for the buffer and 0.23 for acetone).

5.3. Transient effects

We found that pumps with low ion density working liquids demonstrate strong current start-up transients. Fig. 7 shows current transients for all the liquids we used with an applied voltage of 50 V. Fig. 8 shows the normalized results for DI water, methanol and acetone. Current is normalized simply using the minimum, $I_{\min}$, maximum, $I_{\max}$, and measured current levels. Upon application of a potential, pump current quickly rises to a maximum value and gradually decreases to a steady state. Each curve is labeled with its best-fit first order exponential relaxation time constants.[5]

We hypothesize that the (short-term) current transients can be represented as a simple equivalent RC circuit. The resistance value R is dominated by the ohmic character of these liquids. We attribute the capacitance C to polarization of at least a subset of ions in the system. We hypothesize that there are ion species that participate in electrode reactions and ion species that do not. Upon application of electric potential across an EO pump (or an

[5] In separate sets of 30 min experiments using buffer and DI water (not shown here), we also observed up to ∼20% "long-term" decreases in flow rate, and this percent decrease was largest for the low ion density solvents. Although we did not investigate long-term stability in this work, this is an important issue in EO pump development and has been discussed in several recent papers [20,21,41].

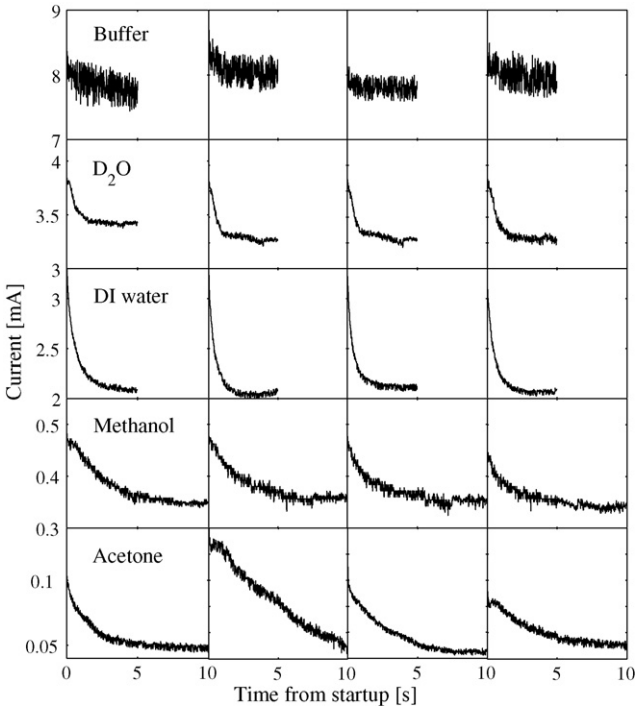

Fig. 7. Time evolution of pump currents with an applied voltage of 50 V for all the working liquids.

electrolytic cell, in general), the latter migrate and polarize the system. The former (reacting species) account for the eventual observed DC current and electroosmotic flow. Presumably, the passive ion species accumulate near electrodes, forming capacitive layers of some thickness δ. We can express the capacitance (per unit area) as $C = \varepsilon/\delta$ and an RC circuit time scale as,

$$\tau_C = \varepsilon L_e/\delta\sigma_\infty, \tag{17}$$

where σ_∞ is the conductivity of the solution and L_e is the distance between electrodes.

A recent paper by Bazant et al. [43] fairly generally treats the problem of charge polarization in the absence of electrode reactions. They studied the dynamics of diffuse charges in EDLs by solving nonlinear Poisson–Nernst–Planck equations. Their

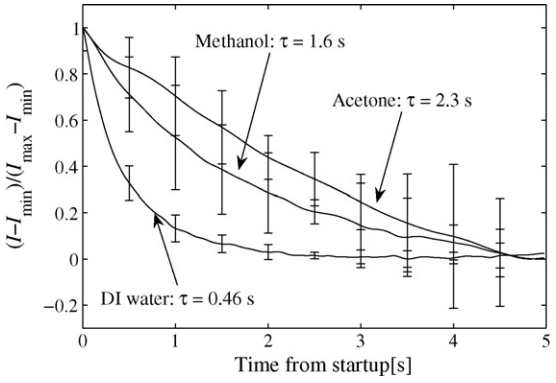

Fig. 8. Time evolution of normalized pump currents with an applied voltage of 50 V for DI water, methanol and acetone. The error bars for flow rate and current were estimated from multiple realizations. The characteristic exponential relaxation time constants also are shown.

Table 3
Time scales for current transients: *RC* circuit time scale and first-order exponential relaxation time scale

	$\tau_C = \varepsilon L_e/\lambda\sigma_\infty$ (s)	$\tau_{(Exp)}$ (s)
Buffer	0.080	0.091
DI water	0.19	0.46
Methanol	0.14, 0.19	1.6
Acetone	0.26, 0.58	2.3

Note: We estimate λ and thus τ_C for methanol and acetone, using two approaches: Scheibel's empirical relation (left-hand column) and Stokes's law with estimated ion size (right-hand column).

model is for a two-component (one positive and one negative ions) electrolyte system. For these systems, δ coincides with Debye length λ, so that $\tau_C = \varepsilon L_e/\lambda\sigma_\infty$ (for nonreacting systems). In our problem (which includes electrode reactions), we do not know if δ scales as λ; however, we can use the ideas presented by Bazant et al. in evaluating the observed trends in the start-up current transients. Table 3 summarizes evaluations of the $\varepsilon L_e/\lambda\sigma_\infty$ time scale, and these are compared to the observed ion current time scales. We use measured values of σ_∞ and the estimates of λ described earlier. We approximate the distance between electrodes for the EO pump as $L_e = L\sqrt{\tau} + 2d$, where L is the porous glass thickness, τ the tortuosity (to account for the effective path length of ions) and d is the distance between each electrode and the surfaces of the pump. For buffer and water, we see that the observed timescales are on the same order as $\varepsilon L_e/\lambda\sigma_\infty$. For methanol and acetone, the observed timescales are about an order of magnitude higher than $\varepsilon L_e/\lambda\sigma_\infty$. This disparity between the aqueous solutions and the organic solvents may contain information regarding the relative content of reacting and nonreacting ions in the system; but it is difficult to make any conclusions. Clearly, a quantitative model for charge polarization in the presence of strong electrolytic reactions is needed to evaluate this issue. As Bazant et al. [43] and Norton et al. [44] point out, however, this complex process is an open problem in electrochemistry. The physics behind these current transients remains an open problem and the role of polarization layers (e.g., by passive ionic species) is an interesting topic for future work.

6. Conclusions

We present an analytical model for EO pumping of low ion density solvents, including organic solvents. The model requires a number of assumptions to estimate ion identity and electrical double layer structure. The model is useful in predicting trends across low conductivity working electrolytes and serves as a basis for system designer optimization. For significant pump loads, the model shows that the optimum value of flow rate per power depends on the specific pump flow rate and pressure load. For example, at $Q = 2$ ml/min, methanol provides higher flow rate per power than acetone for pump loads greater than 0.07 kPa (and lower flow rate per power for smaller loads).

We perform a set of experiments that confirm predicted trends of key figures of merit with varying voltage and also highlight the importance of key parameters including conductivity and double layer thickness relative to pump pore diameter. For neg-

ligible pump loads, we found that flow rate per power is in the decreasing order of acetone, methanol, heavy water, DI water and borate buffer (1 mM sodium concentration), in accordance with the model. Measured flow rate, current and pressure clearly demonstrate finite EDL effects, especially for low ion density liquids. For example, acetone shows about the same EO mobility as buffer, but significantly lower maximum flow rate due to its thick EDL. The finite EDL effects are captured by the predicted values of f and g.

We found strong (short-term) current transients with low ion density liquids. We hypothesize that these may be due to capacitive charge layers near electrodes. Interesting future work in the area of electroosmotic pump development includes developing models for these current transients and practical studies of long-term pump performance.

References

[1] S.H. Yao, J.G. Santiago, J. Colloid Interface Sci. 268 (2003) 133.
[2] V. Pretorius, B.J. Hopkins, J.D. Schieke, J. Chromatogr. 99 (1974) 23.
[3] F. Theeuwes, J. Pharm. Sci. 64 (1975) 1987.
[4] P.K. Dasgupta, S. Liu, Anal. Chem. 66 (1994) 1792.
[5] B.J. Kirby, T.J. Shepodd, E.F. Hasselbrink, J. Chromatogr. A 979 (2002) 147.
[6] L.N. Jiang, J. Mikkelsen, J.M. Koo, D. Huber, S.H. Yao, L. Zhang, P. Zhou, J.G. Maveety, R. Prasher, J.G. Santiago, T.W. Kenny, K.E. Goodson, IEEE Trans. Components Packaging Technol. 25 (2002) 347.
[7] C. Buie, J.D. Posner, T. Fabian, S.W. Cha, D. Kim, F.B. Prinz, J.K. Eaton, J.G. Santiago, J. Power Sources 161 (2006) 191.
[8] D.S. Reichmuth, G.S. Chirica, B.J. Kirby, Sens. Actuators B: Chem. 92 (2003) 37.
[9] S.H. Yao, A.M. Myers, J.D. Posner, K.A. Rose, J.G. Santiago, J. Microelectromech. Syst. 15 (2006) 717.
[10] S.H. Yao, D.E. Hertzog, S.L. Zeng, J.C. Mikkelsen, J.G. Santiago, J. Colloid Interface Sci. 268 (2003) 143.
[11] J.Y. Min, E.F. Hasselbrink, S.J. Kim, Sens. Actuators B: Chem. 98 (2004) 368.
[12] S.K. Griffiths, R.H. Nilson, Electrophoresis 26 (2005) 351.
[13] C. Buie, D. Kim, S. Litster, J.G. Santiago, Electrochem. Soc. (ECS) Trans. 3 (1) (2006) 1279.
[14] M.L. Riekkola, Electrophoresis 23 (2002) 3865.
[15] M. Lammerhofer, J. Chromatogr. A 1068 (2005) 31.
[16] S.P. Porras, E. Kenndler, Electrophoresis 26 (2005) 3203.
[17] P.B. Wright, A.S. Lister, J.G. Dorsey, Anal. Chem. 69 (1997) 3251.
[18] E. Valko, H. Siren, M. Riekkola, J. Microcolumn Sep. 11 (1999) 199.
[19] L. Chen, J. Ma, Y. Guan, J. Chromatogr. A 1028 (2004) 219.
[20] Z. Chen, P. Wang, H.C. Chang, Anal. Bioanal. Chem. 382 (2005) 817.
[21] P. Wang, Z. Chen, H.C. Chang, Sens. Actuators B: Chem. 113 (2006) 500.
[22] J.R. Chipperfield, Non-aqueous Solvents, Oxford University Press, Oxford, 1999.
[23] Y. Marcus, The Properties of Solvents, John Wiley & Sons, New York, NY, 1998.
[24] W.F. Sheehan, Physical Chemistry, Allyn and Bacon, Boston, MA, 1969.
[25] J.H. Moore, N.D. Spencer, Encyclopedia of Chemical Physics and Physical Chemistry, vol. 1–3, Institute of Physics, London, 2001.
[26] S.R. Narayanan, T.I. Valdez, W. Chun, Electrochem. Solid-State Lett. 3 (2000) 117.
[27] S. Kim, N. Koratkar, T. Karabacak, T. Lu, Appl. Phys. Lett. 88 (2006) 263106.
[28] D.R. Lide, CRC Handbook of Chemistry and Physics, 85th ed., CRC Press, Cleveland, OH, 2005.
[29] G. Tchobanoglous, E.D. Schroeder, Water Quality: Characteristics, Modeling, Modification, Addison-Wesley, Reading, MA, 1985.
[30] J.O.M. Bockris, A.K.N. Reddy, Modern Electrochemistry: Ionics, second ed., Plenum, New York, NY, 1998.
[31] http://www.nist.gov/srd/nist1.htm.
[32] C.E. Melton, P.S. Rudolph, J. Chem. Phys. 31 (1959) 1485.
[33] R.T. Aplin, H. Budzikiewicz, C. Djerassi, J. Am. Chem. Soc. 87 (1965) 3180.
[34] E. de Hoffmann, V. Stroobant, Mass Spectrometry: Principles and Applications, second ed., John Wiley and Sons, New York, NY, 2001.
[35] E.G. Scheibel, Ind. Eng. Chem. 46 (1954) 2007.
[36] R.C. Reid, J.M. Prausnitz, T.K. Sherwood, The Properties of Gases and Liquids, third ed., McGraw-Hill, New York, NY, 1977.
[37] R.A. Robinson, R.H. Stokes, Electrolyte Solutions, second ed., Butterworths, London, 1965.
[38] X. Huang, M.J. Gordon, R.N. Zare, Anal. Chem. 60 (1988) 1837.
[39] S.C. Jacobson, J.M. Ramsey, Anal. Chem. 69 (1997) 3212.
[40] J.D. Posner, J.G. Santiago, J. Fluid Mech. 555 (2006) 1.
[41] A. Brask, J.P. Kutter, H. Bruus, Lab on a Chip 5 (2005) 730.
[42] S. Zeng, C.H. Chen, J.C. Mikkelsen Jr., J.G. Santiago, Sens. Actuators B: Chem. 79 (2001) 107.
[43] M.Z. Bazant, K. Thornton, A. Ajdari, Phys. Rev. E 70 (2004) 021506.
[44] J.D. Norton, H.S. White, S.W. Feldberg, J. Phys. Chem. B 94 (1990) 6772.

Biographies

Daejoong Kim received the PhD degree in mechanical engineering at Stanford University, Stanford, California, in 2007. Before that, he earned the BS and MS degrees in mechanical engineering at Seoul National University, Seoul, Korea, in 1999 and 2001, respectively. His graduate research focuses on fundamental studies on electroosmotic flows and development of electroosmotic pumps for miniature fuel cell applications. He is currently a postdoctoral research associate in chemical and biomolecular engineering at the University of Illinois at Urbana-Champaign, working on nanoscale electrokinetics applied for MEMS hydrogen generators.

Jonathan D. Posner received the MS and PhD degrees in mechanical engineering at the University of California, Irvine, in 1998 and 2001, respectively. In addition, he spent 18 months as a fellowship student at the von Karman Institute for Fluid Mechanics in Rhode Saint Genese, Belgium. As a Research Scientist at Neophotonics Corporation he developed an aerosol based, laser pyrolysis nanoparticle reactor for optical films and fuel cell electrolytes. He also spent 2 years as a Postdoctoral Fellow at Stanford University, Stanford, CA, in the Mechanical Engineering Department. He is currently an assistant professor at Arizona State University in the Department of Mechanical and Aerospace engineering. His interests include microscale transport phenomena, fluid dynamics, electrokinetics and optical diagnostics as they apply to the physics and design of micro/nanofluidic bioanalytical and energetic devices. Applications of his research include: novel bioassay functionality, personalized medicine (genome/proteome specific therapy), precision biology, real-time environmental monitoring, drug delivery and fuel cells. Dr. Posner was honored for his excellence in experimental research by the von Karman Institute for Fluid Dynamics and his work has appeared on the cover of *Applied Optics* and the *Journal of Microfluidics and Nanofluidics*.

Juan G. Santiago received the PhD degree in mechanical engineering from the University of Illinois at Urbana-Champaign (UIUC); where he received five fellowships as a doctoral candidate. He was a senior member of the Technical Staff at the Aerospace Corporation (1995–1997). Prof. Santiago received a Ford Foundation Postdoctoral Fellowship (1997), and worked as a Research Scientist at UIUC's Beckman Institute (1997–1998). Santiago is an associate professor in the Mechanical Engineering Department at Stanford. He specializes in microscale transport phenomena, electrokinetics and microfluidic system design. His research includes the optimization and development of novel microsystems for pumping liquids, on-chip electrophoresis, sample concentration methods and miniature fuel cells. The applications of this work include microfabricated bioanalytical systems for genetic analysis, drug discovery, bioweapon detection, drug delivery and power generation. He has received a Frederick Emmons Terman Fellowship (1998–2001); won the National Inven-

tor's Hall of Fame Collegiate Inventors Competition (2001); was awarded the Outstanding Achievement in Academia Award by the GEM Foundation (2006); and was awarded a National Science Foundation PECASE Award (2003–2008). He is an associate editor of the *Journal of Microfluidics and Nanofluidics*, co-founder of Cooligy Inc., co-inventor of micron-resolution particle image velocimetry and director of the Stanford Microfluidics Laboratory. He and his students have been awarded nine best paper and best poster awards. Santiago has given 10 keynote and named lectures and over 100 additional invited lectures. Since 1998, he has graduated 13 PhD students, advised 10 postdoctoral researchers, authored and co-authored 70 archival publications, authored and co-authored 150 conference papers and been awarded 12 patents.